Martin R, Widmer JD, Mecrow BC, Kimiabeigi M, Mebarki A, Brown NL.
Electromagnetic Considerations for a Six-Phase Switched Reluctance Motor Driven by a Three-Phase Inverter.
IEEE Transactions on Industry Applications 2016, 52(5), 3783-3791.

Copyright:

© 2016 IEEE. Personal use of this material is permitted. Permission from IEEE must be obtained for all other uses, in any current or future media, including reprinting/republishing this material for advertising or promotional purposes, creating new collective works, for resale or redistribution to servers or lists, or reuse of any copyrighted component of this work in other works.

DOI link to article:

http://dx.doi.org/10.1109/TIA.2016.2564344

Date deposited:

26/10/2016

Newcastle University ePrints - eprint.ncl.ac.uk

Electromagnetic Considerations for a Six-Phase Switched Reluctance Motor Driven by a Three-Phase Inverter

Richard Martin, James D. Widmer, Barrie C. Mecrow, Mohammad Kimiabeigi, Abdeslam Mebarki, and Neil L. Brown

Abstract—**The Switched Reluctance Machine (SRM) offers advantages over other topologies, but low torque density, high torque ripple, and use of a non-standard power converter are limitations. This paper develops a drive configuration which facilitates the operation of a six-phase SRM using a standard three-phase inverter in order to address these limitations. The focus of the paper is an investigation of electromagnetic design aspects of two candidate SRM topologies in this six-phase context for a pure electric or hybrid electric vehicle type application. Advances are made in the understanding of the electromagnetic design of suitable SRMs, and the conventional SRM is demonstrated as the preferred topology through parametric and FEA design studies with reference to a given specification. Laboratory test results for a prototype machine are presented in verification of the machine design and demonstration of this drive concept as a high torque density candidate suitable for electric vehicle applications.**

Index Terms-- **Motor drives, multiphase electric machines, variable-speed drives, rotating machines, segmental rotor, switched reluctance motor, torque density, torque ripple.**

I. Introduction

SWITCHED Reluctance Machines (SRMs) are currently of considerable interest as an alternative to Permanent Magnet (PM) machines, primarily owing to concerns about price volatility, supply security and environmental impact relating to the highest performing rare-earth PM materials[1-4]. SRMs offer further advantages, namely: cheap, simple and robust construction; absence of cogging torque and open-circuit EMF; and a natural field weakening characteristic which facilitates efficient constant power operation well beyond base speed. The absence of a demagnetization risk means that high temperature operation is a useful possibility.

This work was supported in part by Innovate UK, Cummins Generator Technologies, and Sevcon Ltd.

R. Martin, J.D. Widmer, B.C. Mecrow, and M. Kimiabeigi are with the School of Electrical and Electronic Engineering, Newcastle University, Newcastle-upon-Tyne, UK (e-mail: richard.martin2@ncl.ac.uk).

A. Mebarki and N.L. Brown are with Cummins Generator Technologies, Stamford, UK.

The torque density and efficiency of SRMs is inferior to the highest performing PM machines, although segmental rotor SRMs have been shown to develop improved torque density and efficiency ratings, [4]. SRMs inherently exhibit torque ripple but a range of methods exist for the minimization of this, [5-7]. It is well understood that increasing the number of phases reduces torque ripple but higher phase numbers generally require more switching devices, more connections between motor and drive, and more current sensors, thus giving rise to increased complexity and cost. This is compounded by the fact that dedicated controllers and power converters for SRMs are not readily available, although the use of conventional drives with SRMs is a current research topic, [8-10].

A drive configuration which allows a three-phase SRM to be driven from a three-phase full bridge converter was previously proposed, [8], and this research was later taken to its logical extension by using pairs of antiparallel diodes to drive a six-phase SRM from the same converter, [11]. More recently, different winding configurations have been investigated and an unconventional phase winding connection proposed for use with this three- to six-phase arrangement, [12]. These advances simultaneously address two of the key disadvantages of SRMs (namely torque ripple and the requirement for a non-standard power converter), and it is proposed that this SRM drive is a viable, torque dense alternative to a PM-based solution. The general concept is illustrated in Fig. 1.

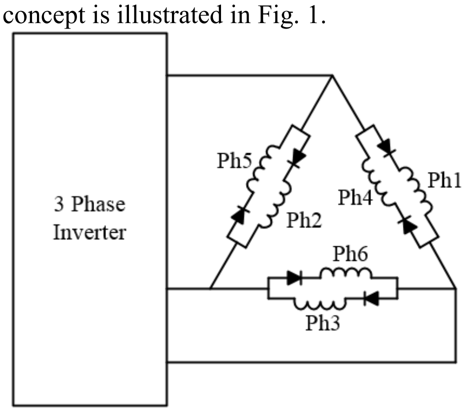

Fig. 1: Concept of driving a six-phase SRM from a three-phase inverter using pairs of antiparallel diodes

This paper, based on a previous conference presentation, [13], develops the three- to six-phase drive configuration through an investigation of the electromagnetic design aspects of six-phase SRMs for use in this context. Two candidate SRM topologies are considered and initial options are compared on the basis of 2D FEA design studies. Performance predictions are given for the preferred topology and the analyses are compared with the results of laboratory tests on a prototype machine.

II. Drive Concept for a Six-Phase SRM

The concept of using pairs of antiparallel diodes to drive a six-phase SRM from a conventional three-phase inverter has been previously reported, [11], and the concept is illustrated in Fig. 1. Six antiparallel diodes convert the bipolar current output from each phase of the three-phase inverter into two unipolar half waveforms, Fig. 2.

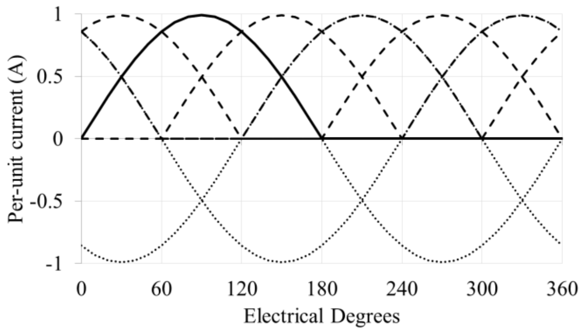

Fig. 2: Idealized current waveforms in the three-phase six-phase drive concept. Three-phase delta currents (dotted line) are rectified to six unipolar pulses (dashed line) suitable for a six-phase SRM. A solid line highlights one such motor phase current.

Consequently the three-phase inverter is able to supply a six-phase SRM, whilst having only three power connections between inverter and motor. In the proposed drive configuration the inverter behaves as though it was supplying a three-phase AC machine and may be configured to supply sinusoidal or quasi-square wave outputs.

As has previously been demonstrated, [11], this drive arrangement offers the following features by comparison with a three-phase SRM more conventionally driven by an asymmetric half bridge converter:

- Standard three-phase inverter drive;
- Only three connections between motor and drive;
- Only two current sensors;
- Low torque ripple;
- No increase in motor loss; and
- Very similar converter VA rating.

A potential shortcoming of the proposed drive is that the phase current tends to a half sinewave instead of a half square wave. However, peak torque is developed in the midrange of a half cycle and the overall effect on the developed torque is minimal.

III. Machine Specification

In designing a prototype six-phase SRM for use with the three-phase full bridge converter drive configuration, a high torque density SRM for use a high temperature environment as part of a pure electric or hybrid electric vehicle drivetrain is envisaged. A nominal specification for this application is summarized in Table 1, and three key operating points are defined in Table 2.

Table 1: Nominal Drive Specification

Peak Torque	650Nm
Continuous Torque	200Nm
Peak Power	75kW
Continuous Power	25kW
Base Speed	1100rpm
Peak Speed	2250rpm
Maximum Lamination Outer Diameter	0.400m
Maximum Stack Length	0.085m
Nominal DC Link Voltage	325V
Maximum Line Current (peak)	550A
Maximum RMS Line Current (continuous)	200A
Maximum Fundamental Frequency (electrical)	1kHz
Coolant Flow Rate	12l/min
Coolant Inlet Temperature	85°C
Maximum Conductor Temperature	200°C

Table 2: Specified ratings at three representative key operating points

Key operating point	A	B	C
Torque (Nm)	110	110	-440
Speed (rpm)	1500	1800	1300
Efficiency	95%	94%	93%

The drive concept set out above is potentially applicable to a range of SRM topologies. For the purposes of this study, a conventional SRM is defined as having simple toothed rotor and stator profiles with each stator tooth carrying a concentrated coil; this topology is well established in the literature as the archetypal SRM. Another contender topology is the segmental rotor SRM; in the single-tooth form, this has a toothed stator with alternate stator teeth carrying concentrated coils, and has been shown to develop up to 65% more torque per unit copper loss than a conventional SRM, [14]. Both topologies are investigated in order to establish the optimal design solution for use with the proposed drive and with regards to the above specification. The general distinction is illustrated, Fig. 3.

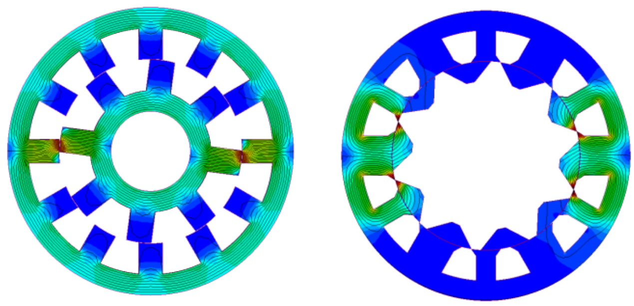

Fig. 3: Distinction between SRM topologies considered: conventional SRM (left) and single-tooth wound segmental rotor SRM (right), each in a three phase topology with a single phase energized

IV. Electromagnetic Design of a Six-Phase Conventional SRM

Electromagnetic design of conventional SRMs is generally well represented in the literature, although six-phase options are uncommon. This section considers the implications of a six-phase conventional SRM.

The maximum average torque output from an SRM, where m is the phase number, N_r is the rotor tooth number, and W' is the co-energy (J), and assuming no phase interaction, is generally given, [15]:

$$T = \frac{mN_r W'}{2\pi} \tag{1}$$

Increasing m and N_r can yield higher torque and torque density, as well as reduced torque ripple through the increased overlap between the actions of adjacent phases, but eventually compromises the co-energy per stroke. In this study, only inner rotor options are considered and, for the avoidance of unbalanced magnetic pull, it is assumed that the stator tooth number options are limited to $2nm$ with n the set of non-zero integers. The electrical angle between adjacent stator coils, where θ_m is the mechanical angle and N_s is the number of stator teeth, is therefore:

$$\theta_e = \theta_m N_r = 360\frac{N_r}{N_s} \tag{2}$$

Thus, the rotor and stator combination must be chosen to give the correct phase displacement for a particular phase number. It is generally desirable to match the stator and rotor tooth width for the avoidance of a zone of constant inductance (which yields no torque), and in the interest of maximizing the inductance ratio this means keeping N_r as close to N_s as possible.

The fundamental electrical frequency is dependent upon the rotor tooth number; consequently, high tooth numbers may give rise to increased iron loss, and the available converter switching frequency may impose a practical limit. Low tooth numbers can bring mechanical disadvantages; for example, large forces of ovalization may arise from topologies with a two-pole field, which could give rise to unacceptable acoustic and mechanical responses.

Where N_s is restricted to $12n$ (for six phases) and θ_e is restricted to 60 or 300 electrical degrees (i.e. ±60, again for six phases), feasible options are shown in Table 3.

Table 3: Feasible tooth combinations for a six-phase conventional SRM

	N_r	
N_s	θ_e=60	θ_e=300
12	14	10
24	28	20
36	42	30
48	56	40

N_r may be given as follows, where the value of n is as previously established:

$$N_r = N_s \pm 2n \tag{3}$$

Generally, $N_r<N_s$, since this maximizes the inductance ratio. The resultant increase in energy converted per loop tends to outweigh the increase in the number of strokes per revolution, [15]. This is particularly true for the higher phase (and consequently tooth) numbers under consideration here owing to the reduced proportional effect on the strokes per revolution. Maximizing the inductance ratio may also may minimize the converter VA requirement, [15], and the potential disadvantages of higher rotor tooth numbers have been mentioned.

From the aforementioned considerations, and in the context of the limits on electrical frequency imposed by the specification, (Table 1), it is clear that a 24:20 topology is the preferred option. In particular, this strikes a compromise between the need to limit the electrical frequency, and avoidance of the two-pole field of the 12:10 option.

The possible coil polarities for a six-phase SRM were examined in an earlier paper, [12]. Conventionally, the two coils of each phase would be connected such that the fluxes reinforce, as shown in Fig. 4. Thus, single-phase energization in the case of the six-phase 12:10 prototype machine would give rise to long flux paths crossing the rotor and utilizing the full rotor core back in the return path. Where the phase number is even, this cannot be realized with a fully symmetric winding. The implications of asymmetry have been investigated, and the realization of a symmetric winding through connection of the phase coils in an unconventional, flux opposing configuration was proposed, [12]. The general distinction is shown in Fig. 4 and this has a number of implications.

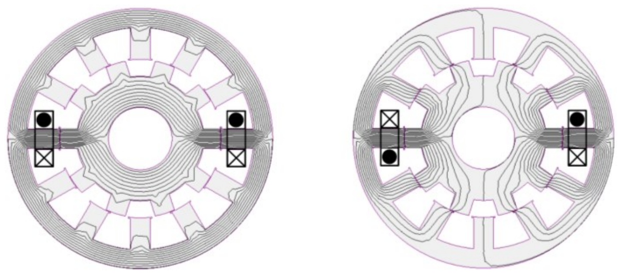

Fig. 4: General distinction between 'reinforcing' coil fluxes (left) and 'opposing' coil fluxes (right) in a six-phase 12-10 SRM with a single-phase energized in the aligned position

Principally, the aligned self-inductance is likely to be reduced owing to the increased reluctance in the magnetic circuit. This will reduce the torque capability but the effect may be offset to some extent by the pronounced mutual coupling between phases. Mutual coupling is often assumed to be negligible in SRM design but can be present in conventional and segmental rotor topologies. Also, the increased reluctance of the flux opposing case reduces the flux per phase and hence allows a commensurate and potentially advantageous reduction in the back iron. Finally, the avoidance of asymmetry in the winding pattern is predicted to reduce torque ripple and redress the average torque capability to some extent.

V. Electromagnetic Design of a Six-Phase Segmental Rotor SRM

Segmental rotor SRMs are well represented in the literature as an alternative SRM topology but have largely been restricted to three-phase variants. Hence, an initial step in this work is to develop generic formulae to enhance understanding of segmental rotor SRMs with alternative phase numbers, and in support of the development of parametric FEA models.

The starting point is the basic electromagnetic circuit and associated design rules set out by Mecrow et al, [16]. The geometric template, Fig. 5, relates the stator tooth pitch, λ_s (m) and rotor segment pitch λ_r (m) at a mean air-gap diameter D_g, (m), to a standard width of flux path *w/2* (m). A consistent gap, *g*, (m), is maintained between adjacent rotor segments and adjacent stator tooth tips for the minimization of the unaligned inductance. This dictates the circumferential dimension of the stator tooth tips and an angle of 45° is assumed for these features.

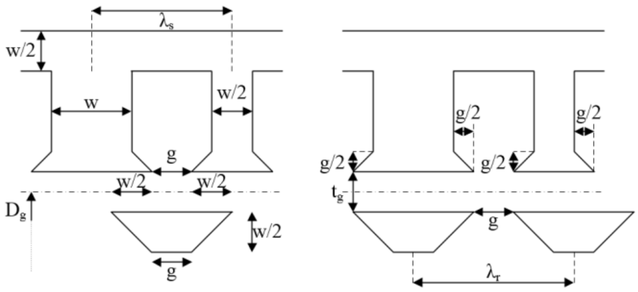

Fig. 5: Basic electromagnetic design parameters for the segmental rotor SRM, showing the rotor segment in the aligned position (left) and unaligned (right)

Ignoring curvature, the design rules are considered in the context of alternative phase numbers, assuming $N_s > N_r$ and $t_g << D_g$, where t_g is the air-gap length. Expressions for rotor segment and stator tooth are first derived:

$$\lambda_r = \frac{\pi D_g}{n_r} = w + 2g \tag{4}$$

$$\lambda_s = \frac{\pi D_g}{n_s} = \frac{3w}{4} + 2g \tag{5}$$

These can then be used to express the parameters *w* and *g* in terms of the mean air-gap diameter and the rotor and stator tooth numbers:

$$w = 4\pi D_g \left(\frac{1}{N_r} - \frac{1}{N_s}\right) \tag{6}$$

$$g = \pi D_g \left(\frac{2}{N_s} - \frac{3}{2N_r}\right) \tag{7}$$

The effective tooth width to rotor pole pitch can be used as a measure of the magnetic utilization of an SRM, [16], and thus an indicator of the specific output. In the case of a conventional SRM, this utilization factor (k_u) is simply the rotor tooth arc to pitch ratio and is generally set between 0.3 and 0.5. Increasing k_u beyond 0.5 soon gives rise to a magnetic short circuit as the rotor teeth starts to overlap adjacent stator teeth, compromising the unaligned inductance. In the case of the segmental rotor SRM, k_u is defined with reference to Fig. 5:

$$k_u = \frac{w}{\lambda_r} \tag{8}$$

Where k_u is less than 0.5, the segmental rotor SRM exhibits a similar aligned flux linkage and a higher unaligned flux linkage by comparison with a conventional SRM [17]. However, maintaining the gap between rotor segments in the unaligned position allows the realization of higher values of k_u without compromising the unaligned inductance. In fact, a value of 0.67 is common in a three-phase machine; almost twice that of a conventional SRM. This superior magnetic utilization can clearly be seen in by inspection of the stator teeth in Fig. 1.

Clearly, the extent to which the advantages of the segmental rotor SRM may be realized is dependent on implementing a high k_u, and, with reference to the geometrical considerations set out above, this can be related to the stator tooth and rotor segment combination:

$$k_u = \frac{w}{\lambda_r} = 4\left(1 - \frac{N_r}{N_s}\right) \tag{9}$$

Assuming the stator teeth are evenly distributed circumferentially in the segmental rotor SRM and applying the previous approach, the alternate tooth winding now gives stator tooth number options of *4mn* and electrical angle between adjacent stator coils of:

$$\theta_e = \theta_m N_r = 360 \frac{N_r}{N_s/2} \tag{10}$$

Feasible options for the segmental rotor SRM are therefore shown in Table 4.

Table 4: Feasible tooth combinations for a six-phase segmental rotor SRM

	N_r	
N_s	θ_e=60	θ_e=300
24	26	22
48	52	44
72	78	66

Where N_r<N_s (for the reasons set out in section IV), the closest suitable N_r may also be given in a similar manner to the conventional SRM:

$$N_r = N_s - 2n \tag{11}$$

This has a number of implications for the segmental rotor SRM design. Firstly, equation (9) for the utilization factor becomes:

$$k_u = 4\left(1 - \frac{N_r}{N_s}\right) = \frac{2}{m} \tag{12}$$

This confirms that the utilization factor, hence the extent to which the advantages of the segmental rotor SRM may be realized where the design rules are followed strictly, is determined by the phase number. Critically, the standard three-phase variant exhibits the high utilization factor previously reported, whereas the six-phase variant exhibits a factor in the range where the conventional SRM is preferable as previously described.

One conclusion could be that the strict design rules are suboptimal for segmental rotor SRMs at higher phase numbers. Attempts were made to address this by systematically relaxing the less critical design constraints, applying similar algebra to the above, and forcing the utilization factor to the value of 0.67 exhibited by high performing three-phase variants. For example, the unwound (thin) tooth is generally set by the design rules, [16], to be half the width of the wound tooth in sensible sizing of the basic flux path. However, if this width is allowed to vary as a proportion of the width of the wound tooth, the resultant design freedom facilitates a choice of utilization factor. In the six-phase case, a utilization factor of 0.67 requires the unwound tooth to be three-quarters of the width of the wound tooth (approximately 50% wider than required) to the detriment of the electrical loading of the machine as the winding slot area is reduced.

Critically, with regard to the specification considered here, none of the theoretically possible segmental rotor SRM tooth combinations are entirely satisfactory, with the minimum 24 stator tooth machine developing an effective two-pole field and any larger tooth number machine exceeding the specified maximum fundamental electrical frequency. However, for comparison with the conventional SRM, the 24:22 and 48:44 options are developed further.

VI. Choice of Topology for a Prototype Six-Phase SRM

Concept designs for the candidate topologies identified in the preceding sections were developed through a combination of manual design work and FEA, including some preliminary optimization of the lamination geometries for the maximization of peak torque. 2D dynamic FEA was used for comparable performance evaluation of the topologies under consideration. Key performance predictions of concept designs on the basis of 2D FEA are shown in Table 5, with a focus on the performance at the operating points as defined in Table 2. Torque ripple is defined here as the peak to peak ripple expressed as a percentage of the mean torque.

Table 5: Summary of concept designs and performance predictions with reference to key operating points A, B, C (Table 2)

Topology		Conventional	Segmental Rotor	Segmental Rotor
Tooth Combination		24:20	24:22	48:44
Number of Coils		24	12	24
Turns per Coil		24	27	14
Peak Torque (Nm)		625	556	518
Torque Ripple	A	48%	36%	35%
	B	48%	36%	36%
	C	22%	17%	14%
Copper Loss (W)	A	528	568	1325
	B	530	570	1331
	C	3698	3526	6956
Iron Loss (W)	A	707	506	571
	B	923	663	760
	C	1122	1033	1299
Efficiency	A	93%	94%	90%
	B	94%	95%	91%
	C	93%	93%	88%

These predictions form the basis of comparison between the topologies and choice of topology for detail design and prototyping. It is clear that none of the options meet the specified target of 650Nm torque. Critically, the conventional SRM comes closest and both versions of the segmental rotor SRM fall quite short of the target. This is in accordance with the preceding electromagnetic analyses which reasoned that the segmental rotor topology offers significant advantages in a three-phase arrangement, but that these advantages are not manifest at higher phase numbers.

From an efficiency perspective, the 48:44 segmental rotor SRM appears to be an outlier with heavy copper loss contributing to inferior efficiency across the key operating points. There is little else to distinguish between the other options expect for a tentative observation that the 24:22 segmental rotor SRM is consistently the most efficient by a small margin.

Hence, the 24:20 conventional SRM is the chosen candidate for prototyping; this is on the primary basis of coming closest to the specified torque requirement. In addition to the torque shortfall, both segmental rotor SRM options have other disadvantages as previously described.

VII. Design and Optimization of a Prototype Six-Phase Conventional SRM

The detail design of a prototype machine incorporates considerable optimization work on the lamination geometry with a view to more closely meeting the specification. This is implemented using the Infolytica MagNet and OptiNet FEA package to couple 2D transient with motion FEA studies to an evolutionary algorithm-based optimization. This approach requires the user to define parametric FEA models along with objective, constraint, and dependency functions. The optimization then uses successive FEA solves to converge on the optimal solution. The parametric lamination templates are shown in Fig. 6.

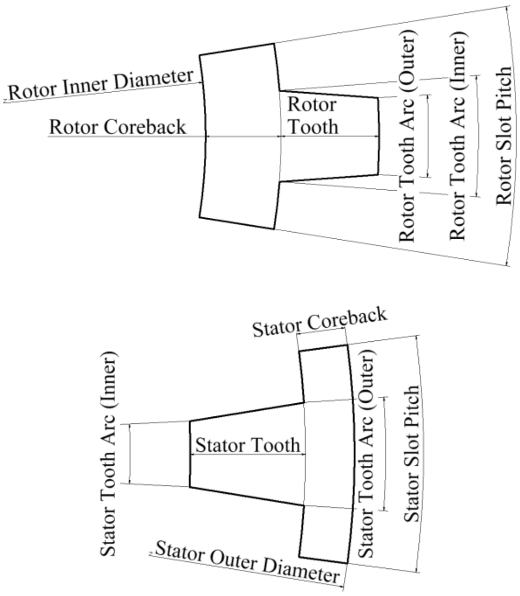

Fig. 6: Parametric lamination templates for 2D FEA optimization, showing rotor (top) and stator (bottom)

Objective functions were varied over a number of optimization runs to include maximization of efficiency and minimization of torque ripple. The concept design work indicates that peak torque is demanding and so the majority of optimization effort focused on maximization of this at base speed. Copper loss is dominant at base speed, peak torque and so the coil MMF was set for each design variation on the basis of a fixed copper loss and fill factor. The laminations are compared pre- and post-optimization in Fig. 7.

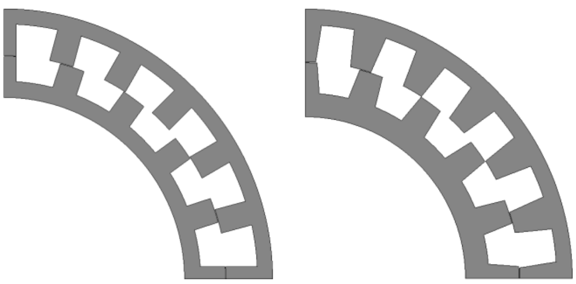

Fig. 7: Lamination templates pre- (left) and post-optimization (right)

Dynamic 2D FEA is used to give a prediction of the capability of the machine and simulations were run across the full operating range of the machine. Switch-on angle (in electrical degrees advanced of the unaligned position) is selected to maximize the torque per amp; a standard inverter drive can vary the current angle with position feedback. A sample 2D MagNet mesh is shown in Fig. 8.

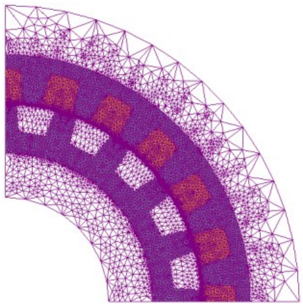

Fig. 8: Final lamination detail design and MagNet 2D FEA mesh for the 24:20 conventional SRM prototype

Performance predictions comparing pre- and post-optimization are shown in Table 6. Significant improvements are evident, and the post-optimization figures compare well with the specification (Table 1), although the practically achievable peak torque is expected to be lower owing to the limitations of 2D FEA.

Table 6: Performance predictions pre- and post-optimization with reference to key operating points A, B, C (Table 2)

		Pre-Optimization	Post-Optimization
Peak Torque (Nm)		625	674
Torque Ripple	A	48%	40%
	B	48%	40%
	C	22%	15%
Copper Loss (W)	A	528	580
	B	530	585
	C	3698	3418
Iron Loss (W)	A	707	450
	B	923	593
	C	1122	803
Efficiency	A	93%	94%
	B	94%	95%
	C	93%	93%

The resulting efficiency map is shown in Fig. 9 in comparison with the torque-speed specification.

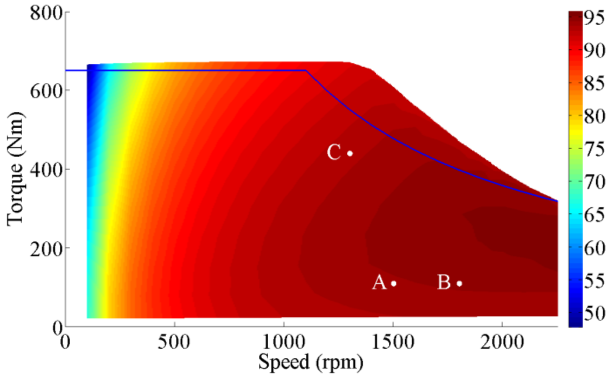

Fig. 9: 2D FEA predicted torque/speed operating range shaded for efficiency (%) showing the specification (blue line) and the key operating points A, B, C as defined in Table 2

Fig. 10 compares various current waveforms in the drive at peak current, base speed, with the phase coils connected in parallel and the machine in delta, all obtained from 2D FEA.

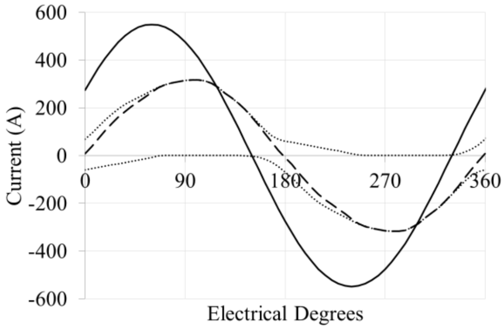

Fig. 10: Instantaneous current waveforms at peak torque, base speed showing back-to-back motor phase currents 1 and 4 (dotted), resultant delta leg current (dashed) and line current (solid)

For maximum torque per amp at this point, the “switch-on” angle of the motor phase current coincides with the unaligned position of the respective phase; the line current can be seen to be sinusoidally controlled to the peak value of 550A and hence the motor is effectively in “current control” here. Although some circulation around the diode pair can be observed, the simulated currents bear close resemblance to the idealized waveforms of Fig. 2. The accompanying instantaneous torque prediction is illustrated in Fig. 11, which indicates an average value of 674Nm and a torque ripple of 9.1%.

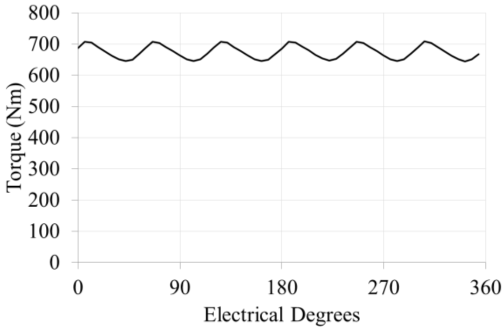

Fig. 11: Instantaneous torque waveform for the prototype design from 2D dynamic FEA at peak torque, base speed

At higher speeds, the switch on angle for the incoming phase can be advanced to maximize the torque, and a region of voltage control occurs above base speed. Given the delta connection and the antiparallel diodes, the individual motor phase currents are less controlled than with an asymmetric half bridge, but clearly the inverter line voltage is the motor phase voltage. Hence, for a given diode pair, the voltage applied to build up current in one phase is equally applied to de-flux its antiparallel partner.

VIII. Experimental Test Results

A prototype machine has been built and tested in the laboratory. The static rig is shown in Fig. 12. This rig enabled the rotor to be locked in various positions with facility for fine tuning the angle for the purpose of static flux linkage measurements.

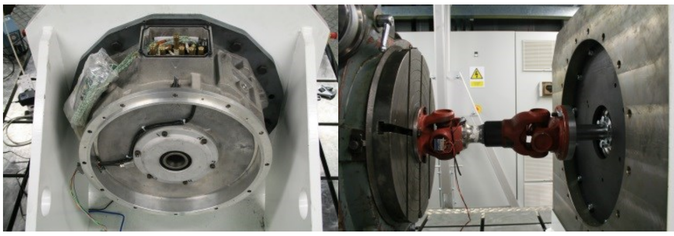

Fig. 12: Static test rig setup showing mounted machine assembly (left) and the cardan shaft connecting the machine to a vertically mounted rotary table (right)

The resultant magnetization characteristics are shown for the aligned and unaligned rotor positions, for a given phase and rotor tooth, in comparison with the FEA predictions, Fig. 13.

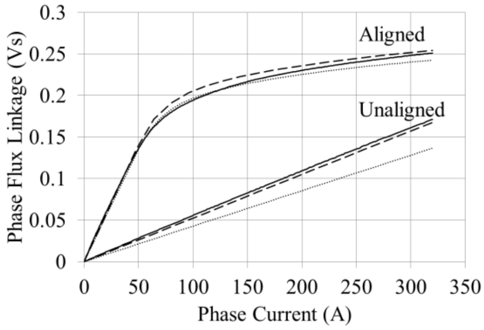

Fig. 13: Results from per phase static flux linkage test (solid lines) compared with 2D FEA (dotted line) and 3D FEA (dashed line)

2D FEA ignores end-leakage and thus under-predicts the unaligned inductance by almost 20%. 3D FEA predictions compare well with experimental results, with the slight under-prediction in the aligned position ascribed to a combination of material variation from data sheet and experimental error.

The measured torque versus RMS line current is shown in Fig. 14, which compares 2D FEA predictions with the test results.

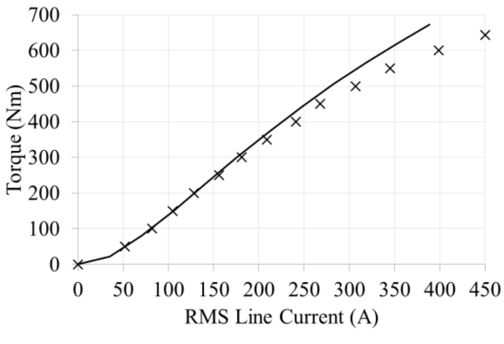

Fig. 14: Torque versus RMS line current from 2D FEA (solid line) compared with the measured performance of the prototype (markers)

The results compare well, allowing for the expected over prediction of 2D FEA. This is particularly evident at higher current levels as the machine saturates and leakage effects become prominent. Clearly the peak torque performance is good; the torque density (stack outer dimensions) exceeds 60Nm/liter, comparable to some of the highest performing SRMs in the current literature, [18].

Fig. 15 illustrates a motor phase current, comparing 2D FEA prediction with an oscilloscope trace from experimental test. This illustrates the resultant motor phase current arising from diode rectification of the inverter input and may be compared with the illustration of the general principle in Fig. 10. However, for ease of measurement, the comparison in Fig. 15 is for continuous operation at 25kW, 1100rpm (base speed).

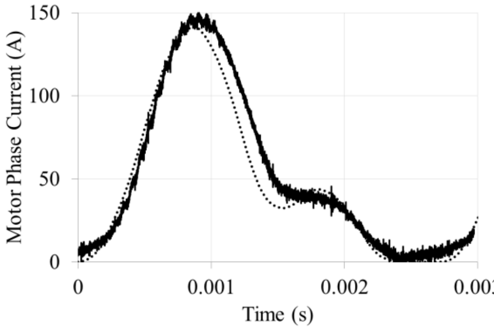

Fig. 15: Motor phase current from 2D FEA (dotted line) compared with an oscilloscope trace from experimental test (solid line) at 25kW, 1100rpm

To complete the picture, Fig. 16 shows the FEA predictions for a phase pair, a leg of the delta connection, and a feeder line current for this operating point.

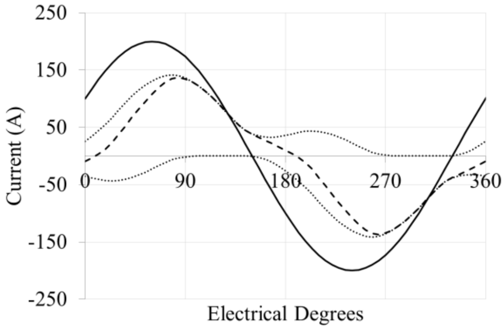

Fig. 16: Instantaneous current waveforms at continuous power, base speed showing back-to-back motor phase currents 1 and 4 (dotted), resultant delta leg current (dashed) and line current (solid)

Efficiency measurement is the subject of continued investigation owing to the difficulty in separating out the components of loss relating to the inverter, diodes and motor. System efficiency was measured by comparing mechanical power output with the DC bus input power, and motor/diode efficiencies were then inferred by using the inverter manufacturer's detailed knowledge of inverter performance under different operating conditions. Results are shown in comparison with the specification, where relevant, and 2D FEA predictions, Table 7.

Table 7: Efficiency results with reference to peak torque and key operating points A, B, C (Table 2)

		Specification (no diodes)	2D FEA (no diodes)	Test (motor + diodes)
Peak Torque (Nm)		N/A	90%	85%
Key Operating Points	A	95%	94%	93%
	B	94%	95%	95%
	C	93%	93%	90%

It must be noted that experimental error in efficiency measurement with this method is likely to be of the order of +/-2%; over- and under-predictions with respect to test evidence this variability. However, efficiencies show a reasonable agreement and the design comes close to meeting the specification in this regard. In general terms, operating efficiencies in the low- to mid- 90% range compare well with what might be expected from a more conventional asymmetric half bridge converter driven SRM.

IX. Conclusions

This paper developed the idea of driving a six-phase SRM from a 3-phase full bridge converter using an unconventional winding configuration previously proposed. Two SRM topologies have been considered and the understanding of electromagnetic design aspects for both topologies has been advanced in the six-phase context. Particular consideration has been given to suitable tooth and segment combinations for use with the proposed drive configuration.

In this design study it was demonstrated that the conventional SRM gives superior torque density and that the segmental rotor SRM topology suffers from sub-optimal magnetic circuit characteristics at this high phase number. This was demonstrated analytically and verified through FEA based comparison of three concept designs.

A conventional, 24:20 SRM was selected as the choice candidate for detail design work. This involved optimization of the electromagnetic design followed by the fabrication of a prototype machine. Test results showed that the machine performs well in comparison with FEA predictions and the initial specification. The high torque density achieved in experimental test particularly recommends this drive configuration as a strong candidate for electric vehicle applications.

X. Acknowledgments

The authors gratefully acknowledge the contributions of the following: Dr Peter Barrass, Steve Savage and Dr Howard Slater of Sevcon Ltd.; Muhammad Awais, Richard Gray and Tanmay Pathak of Cummins Generator Technologies; and the staff of the mechanical workshop, School of Electrical and Electronic Engineering, Newcastle University.

References

[1] A. Chiba, Y. Takano, M. Takeno, T. Imakawa, N. Hoshi, M. Takemoto, *et al.*, "Torque Density and Efficiency Improvements of a Switched Reluctance Motor Without Rare-Earth Material for Hybrid Vehicles," *Industry Applications, IEEE Transactions on,* vol. 47, pp. 1240-1246, 2011.

[2] D. G. Dorrell, A. M. Knight, L. Evans, and M. Popescu, "Analysis and Design Techniques Applied to Hybrid Vehicle Drive Machines-Assessment of Alternative IPM and Induction Motor Topologies," *Industrial Electronics, IEEE Transactions on,* vol. 59, pp. 3690-3699, 2012.

[3] H. Yihua, S. Xueguan, C. Wenping, and J. Bing, "New SR Drive With Integrated Charging Capacity for Plug-In Hybrid Electric Vehicles (PHEVs)," *Industrial Electronics, IEEE Transactions on,* vol. 61, pp. 5722-5731, 2014.

[4] J. D. Widmer, R. Martin, and B. C. Mecrow, "Optimization of an 80-kW Segmental Rotor Switched Reluctance Machine for Automotive Traction," *Industry Applications, IEEE Transactions on,* vol. 51, pp. 2990-2999, 2015.

[5] N. C. Sahoo, J. X. Xu, and S. K. Panda, "Low torque ripple control of switched reluctance motors using iterative learning," *Energy Conversion, IEEE Transactions on,* vol. 16, pp. 318-326, 2001.

[6] I. Husain, "Minimization of torque ripple in SRM drives," *Industrial Electronics, IEEE Transactions on,* vol. 49, pp. 28-39, 2002.

[7] N. T. Shaked and R. Rabinovici, "New procedures for minimizing the torque ripple in switched reluctance motors by optimizing the phase-current profile," *Magnetics, IEEE Transactions on,* vol. 41, pp. 1184-1192, 2005.

[8] A. C. Clothier and B. C. Mecrow, "The use of three phase bridge inverters with switched reluctance drives," in *Electrical Machines and Drives, 1997 Eighth International Conference on (Conf. Publ. No. 444)*, 1997, pp. 351-355.

[9] P. Somsiri, K. Tungpimonrut, and P. Aree, "Three-phase full-bridge converters applied to switched reluctance motor drives with a modified switching strategy," in *Electrical Machines and Systems, 2007. ICEMS. International Conference on*, 2007, pp. 1563-1568.

[10] X. Liu, Z. Q. Zhu, M. Hasegawa, A. Pride, R. Deodhar, T. Maruyama*, et al.*, "Performance comparison between unipolar and bipolar excitations in switched reluctance machine with sinusoidal and rectangular waveforms," in *Energy Conversion Congress and Exposition (ECCE), 2011 IEEE*, 2011, pp. 1590-1595.

[11] J. D. Widmer, B. C. Mecrow, C. M. Spargo, R. Martin, and T. Celik, "Use of a 3 phase full bridge converter to drive a 6 phase switched reluctance machine," in *Power Electronics, Machines and Drives (PEMD 2012), 6th IET International Conference on*, 2012, pp. 1-6.

[12] J. D. Widmer, R. Martin, C. M. Spargo, B. C. Mecrow, and T. Celik, "Winding configurations for a six phase switched reluctance machine," in *Electrical Machines (ICEM), 2012 XXth International Conference on*, 2012, pp. 532-538.

[13] R. Martin, J. D. Widmer, B. C. Mecrow, M. Kimiabeigi, A. Mebarki, and N. L. Brown, "Electromagnetic considerations for a six-phase switched reluctance motor driven by a three-phase inverter," in *2015 IEEE International Electric Machines & Drives Conference (IEMDC)*, 2015, pp. 280-286.

[14] J. D. Widmer and B. C. Mecrow, "Optimized Segmental Rotor Switched Reluctance Machines With a Greater Number of Rotor Segments Than Stator Slots," *Industry Applications, IEEE Transactions on,* vol. 49, pp. 1491-1498, 2013.

[15] T. J. E. Miller, *Switched Reluctance Motors and Their Control*: Magna Physics, 1993.

[16] B. C. Mecrow, E. A. El-Kharashi, J. W. Finch, and A. G. Jack, "Segmental rotor switched reluctance motors with single-tooth windings," *Electric Power Applications, IEE Proceedings -,* vol. 150, pp. 591-599, 2003.

[17] B. C. Mecrow, J. W. Finch, E. A. El-Kharashi, and A. G. Jack, "Switched reluctance motors with segmental rotors," *Electric Power Applications, IEE Proceedings -,* vol. 149, pp. 245-254, 2002.

[18] A. Chiba, K. Kiyota, N. Hoshi, M. Takemoto, and S. Ogasawara, "Development of a Rare-Earth-Free SR Motor With High Torque Density for Hybrid Vehicles," *Energy Conversion, IEEE Transactions on,* vol. 30, pp. 175-182, 2015.

Richard Martin received the MEng degree in general engineering (2002) and PhD degree in electrical engineering (2007) from the University of Durham, UK. He is a Senior Research Associate with Newcastle University, UK and his interests include the electromagnetic design of permanent magnet and switched reluctance machines.

James D. Widmer has a PhD in the design of electrical machines from Newcastle University, UK. He joined Newcastle University in 2009 from a senior post in the aerospace industry. He is responsible for the “Centre for Advanced Electrical Drives” at Newcastle University which works with industry partners to convert academic research into world-class products. His research interests include high-efficiency permanent magnet machines and rare-earth magnet-free motor topologies.

Barrie C. Mecrow received the PhD degree from Newcastle University, UK. He commenced his career as a Turbogenerator Design Engineer with NEI Parsons, Newcastle upon Tyne, UK. He became a Lecturer in 1987 and a Professor in 1998 with Newcastle University. He is the Head of the School of Electrical and Electronic Engineering at Newcastle University where he is also a Professor of electrical power engineering. His research interests include fault-tolerant drives, high-performance permanent-magnet machines, and novel switched reluctance drives.

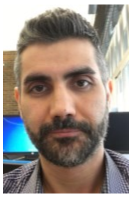

Mohammad Kimiabeigi received the M.S. degree in electric power engineering from the Royal Institute of Technology, Sweden, in 2008, and is currently working toward PhD at Newcastle University, UK. He has worked as a research engineer at the ABB competence centre in Sweden, Siemens Wind Power headquarter in Denmark, and Siemens Wind Power competence centre in the UK. Mr Kimiabeigi holds 12 granted European and U.S. patents and more than 20 filed inventions in the field of electrical drives for the renewable sectors.

Abdeslam (Salem) Mebarki received his PhD degree in Electrical and Electronic Engineering from the University of Bath, UK in 1994. From 1996 to 2000 he was with Westwind Air Bearings Ltd. In 2000 he joined the R&T team at Cummins Generator Technologies, Stamford, UK, as Electromagnetic Design Engineer. Currently he is a Technical Project Leader, leading projects on the design and development of novel electrical motors/generators for applications such as HEV, high speed machines for the more electric engine, renewables and power generation. His research interests include electrical machines design, development and control, and multi-physics simulation and modelling.

Neil L. Brown received his PhD degree in Novel Electrical Machines (2002) from the University of Durham, UK. He is Director of Research and Technology at Cummins Generator Technologies, visiting Professor at the University of Nottingham, and a Fellow of the Institute of Engineering and Technology.